Transition metal (TM = V, Cr, Mn, Fe, Co, Ni)-doped GeSe diluted magnetic semiconductor thin films with high-temperature ferromagnetism

Deren Li[1], Xi Zhang[1*], Wenjie He[1], Yong Peng[2] and Gang Xiang[1*]

ABSTRACT Group-IV metal chalcogenides-based diluted magnetic semiconductor (DMS) thin films with high-temperature ferromagnetism (FM) are desirable for semiconductor spintronic devices. In this paper, transition-metal (TM = V, Cr, Mn, Fe, Co and Ni)-doped GeSe polycrystalline films are deposited by solid-source chemical vapor deposition (CVD). Magnetic measurements reveal that Mn-, Fe- and Co-doped GeSe films exhibit robust FM with Curie temperatures (T_C) up to 277, 255 and 243 K, respectively, whereas V-, Cr- and Ni-doped GeSe films show weak FM. Magneto-transport measurements show that Mn-, Fe- and Co-doped GeSe films possess relatively high hole concentrations up to $\sim 10^{20}$ cm^{-3} at 300 K. Further analysis based on experimental and calculation results shows that the robust FM in Mn-, Fe- and Co-doped GeSe films is attributed to the carrier-enhanced Ruderman-Kittel-Kasuya-Yosida interaction. Our results give insights into the rich variety in TM-doped GeSe DMS thin films and offer a new platform for related fundamental research and device applications.

Keywords: Group IV metal chalcogenides, IV-VI diluted magnetic semiconductor, TM-doped GeSe, high-temperature ferromagnetism, chemical vapor deposition

INTRODUCTION

Group IV metal chalcogenides (metal = Ge, Sn; chalcogen = S, Se, Te)-based diluted magnetic semiconductors (DMSs), or IV-VI DMSs, a group of novel functional materials integrating magnetic and semiconducting properties simultaneously, are promising candidates for semiconducting spintronic and electronic devices [1]. The ferromagnetic transition temperature, i.e., Curie temperature (T_C), has been extensively investigated to meet the requirement of practical applications at room temperature (RT) [2–7], because the T_C of a DMS indicates the upper bound of working temperature for the DMS-based materials and devices [8–10]. In early times, IV-VI DMSs such as $Pb_{1-x-y}Sn_yMn_xTe$ and $Sn_{1-x}Mn_xTe$ crystals were grown using molecular beam epitaxy (MBE) and exhibited T_C up to 6 K [11,12]. In 2017, Li *et al.* [13] reported that the Fe-doped SnS_2 monolayer prepared by mechanical exfoliation shows a T_C of ~31 K. Recently, other IV-VI DMSs such as $Ge_{1-x}Cr_xTe$ [14], $Ge_{1-x}Mn_xTe$ [1], and $Ge_{1-x}Fe_xTe$ [15] films with T_C up to 160 K

have been fabricated by various methods including MBE, pulsed laser deposition (PLD) and magnetron sputtering method. Two-dimensional (2D) van der Waals (vdW) IV-VI DMSs such as layered Fe_3GeTe_2 [16], five-layer $CrGeTe_3$ [17], and few-layer $CrSiTe_3$ [18] with T_C of 211, 65 and 120 K, respectively, have also been fabricated by standard ampule technique, mechanical exfoliation, and mechanical cleavage method, respectively. Meanwhile, theoretical work predicted that the T_C values in $CrSnTe_3$ [19], $Cr_2Ge_2Te_6$ [20] and $Cr_2Si_2Te_6$ [20] monolayers can reach 170, 108 and 111 K, respectively. Nevertheless, low T_C values far below RT and complex preparation methods are still the main obstacles for practical applications of IV-VI DMSs. Recently, there have been some reports on transition-metal (TM)-doped GeSe magnetic semiconductors. In 2018, Yang *et al.* [21] predicted that magnetism could be induced in GeSe by most of 3d TM ions except TM = Sc, Ti, Cu, Zn. In 2019, Mao *et al.* [22] found that the zigzag GeSe nanoribbon with odd-number P atoms substitutional doping at edges could exhibit ferromagnetism (FM) with magnetic moment of 1 μ_B. In 2020, Shu *et al.* [23] theoretically demonstrated that Fe-, Co-, and Ni-doped GeSe exhibited FM with magnetic moments of 4.00 μ_B, 2.96 μ_B, and 1.91 μ_B, respectively. However, these reports were theoretical but not experimental results. Very recently, our work has shown that comb-structured Mn-doped GeSe nanostructures exhibit a high T_C of 309 K owing to the combined effect of Ruderman-Kittel-Kasuya-Yosida (RKKY) interaction, crystalline ordering and shape anisotropy [24]. Compared with other forms of ferromagnetic materials, ferromagnetic thin films are compatible with the mainstream thin-film based device applications, which means that the design, fabrication and application of the ferromagnetic thin films can be easily integrated with the current thin film technologies [8]. However, the discontinuous GeSe nanostructures are not compatible with mainstream thin-film based device applications; indeed, high-T_C IV-VI DMSs thin films doped with various TM elements are more expected.

Based on the above facts, we have fabricated homogeneous TM (TM = V, Cr, Mn, Fe, Co and Ni)-doped GeSe (GeTMSe) films *via* one-step chemical vapor deposition (CVD), and studied their structures and magnetic and transport properties. All the obtained GeTMSe samples show FM. Specifically, the GeMnSe, GeFeSe and GeCoSe films show robust FM with T_C up to 277, 255 and 243 K, respectively, unveiling new opportunities in group IV metal chalcogenides-based DMS films for spintronic

[1] College of Physics, Sichuan University, Chengdu 610064, China
[2] College of Physical Science and Technology, Lanzhou University, Lanzhou 730000, China
* Corresponding authors (emails: xizhang@scu.edu.cn (Zhang X); gxiang@scu.edu.cn (Xiang G))

applications.

EXPERIMENTAL SECTION

Materials and methods

Various TM atoms (V, Cr, Mn, Fe, Co, and Ni)-doped GeSe films were grown by CVD, in which GeSe and corresponding metal salt (VCl_3, $Cr(CH_3COO)_3$, $MnCl_2$, $FeCl_2$, $CoCl_2$ and $Ni(CH_3COO)_2$, respectively) powders with appropriate amounts were used as the raw materials. The reactants were placed in a quartz tube filled with a forming gas (5% H_2 + 95% Ar). The precursor powders were evaporated in the high temperature zone (750–800°C) and then precipitated in the low temperature zone (250–300°C) of the tubular furnace. A more detailed preparation flowchart and the doped atomic structure diagram are given in Fig. 1.

Characterizations

The films' morphologies, microstructures and chemical compositions were explored with scanning electron microscopy (SEM, JSM-5900 LV), atomic force microscopy (Benyuan, CSPM5500), X-ray diffractometer (XRD, Fangyuan, DX-2500) equipped with a Cu-Kα radiation (λ = 0.154 nm), Raman spectrometer (LabRAM HR) with an excitation wavelength of 532 nm, and transmission electron microscopy (TEM, FEI Tecnai G2 F30). X-ray photoelectron spectrometer (XPS, AXIS Ultra DLD (Kratos)) was used to explore the elemental composition and chemical valence states of films. The electron paramagnetic resonance (EPR) measurements were carried out on a Bruker X-band spectrometer (EMX-PLUS) equipped with a continuous flow cryostat at the temperature of T = 300 K. Magnetization measurements were performed on a superconducting quantum interference device (SQUID, Quantum Design MPMS-XL-5). To obtain a van der Pauw structure for transport measurements, metallic contacts of 50-nm-thick Au were deposited by thermal evaporation with a shadow mask and annealed at 500°C under N_2 for 60 s. Transport measurements
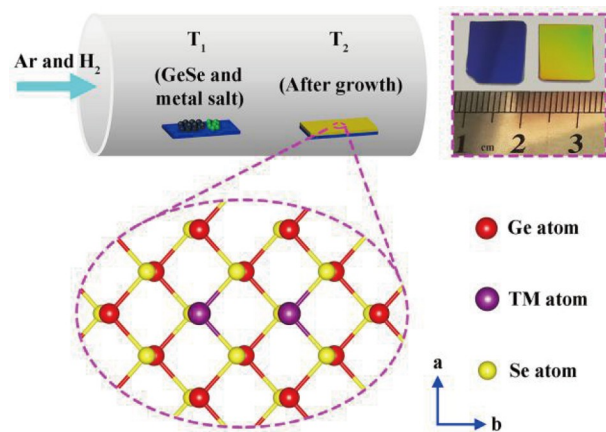

Figure 1 Schematic illustration of the fabrication procedures and the doped atomic structure diagram for GeTMSe films.

were conducted in a physical property measurement system (PPMS-9, Quantum Design) under a magnetic field up to 3 T.

Theoretical calculations

The Vienna *ab initio* simulation package (VASP) was employed for the first-principles calculations based on the density functional theory (DFT) [25]. The projector-augmented wave (PAW) potentials and the generalized gradient approximation (GGA) of Perdew-Burke-Ernzernhof (PBE) were utilized to describe the exchange and correlation potentials. The calculations were carried out with the cut-off energy of 500 eV to ensure the expansion of wave function into plane waves. In order to fully optimize the initial geometry structures, the convergence criteria were set as 0.01 eV Å^{-1} in force and 10^{-5} eV in energy. The 15 Å vacuum layer was selected to avoid interlayer interactions between adjacent supercells. In the self-consistent field and total energy calculations, the Brillouin zone samplings were done by 13 × 1 × 1 Monkhorst-Pack k-point. To reasonably describe the
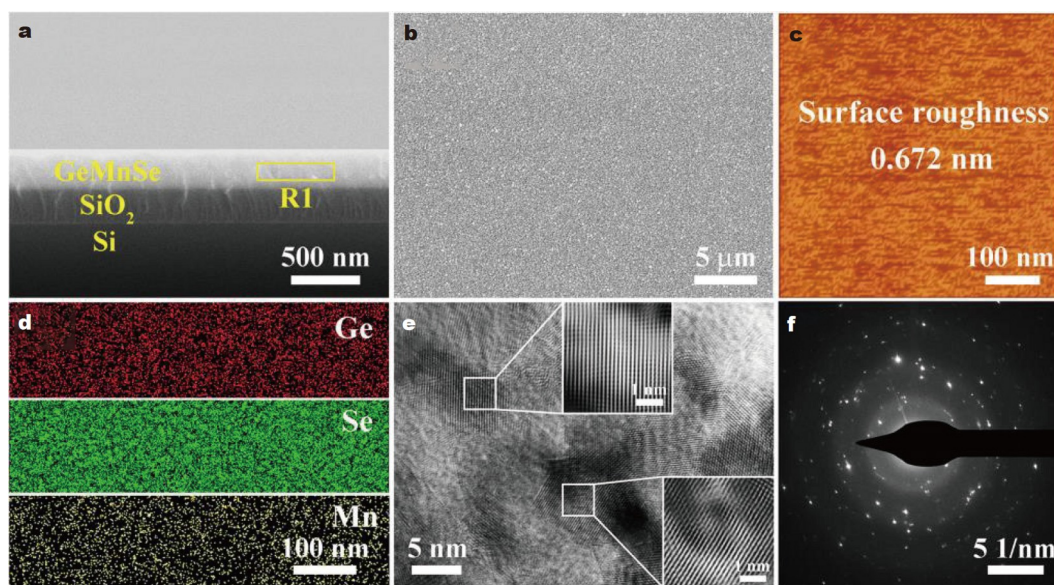

Figure 2 (a) Cross-sectional SEM image of the GeMnSe film/SiO₂/Si substrate. (b) Top surface SEM image and (c) atomic force microscopy image of the GeMnSe film. (d) EDS elemental mappings of the R1 region in (a). (e) HRTEM image and (f) SAED pattern of the GeMnSe film. The insets in (e) are the zoomed-in pictures of the selected square areas.

relevant interactions of 3d electrons of the TM (TM = V, Cr, Mn, Fe, Co, and Ni) atoms, GGA+U (U = 3 eV) calculations were employed to investigate the magnetic properties [26].

RESULTS AND DISCUSSION

The microscopic images of a typical GeMnSe film are shown in Fig. 2. In fact, all the other GeTMSe films show similar morphologies and microstructures (Figs S1–S5). Fig. 2a shows the cross-sectional SEM image of 300-nm-thick GeMnSe film/SiO$_2$/Si substrate, and Fig. 2b shows the uniform smooth surface of the GeMnSe film. The energy dispersive spectroscopy (EDS) spectra show that the TM composition x in the Ge$_{1-x}$TM$_x$Se film is about 1.0 at.% (Fig. S6), which is consistent with subsequent XPS results. The atomic force microscopy surface profile in Fig. 2c shows that the GeMnSe film surface roughness is around 0.672 nm. Fig. 2d shows the elemental mappings of the R1 region in Fig. 2a, which indicates the incorporation and the uniform distribution of Mn ions in the GeMnSe thin film. Fig. 2e shows the high-resolution TEM (HRTEM) image of the GeMnSe film, where the different crystalline orientations and obvious lattice fringes are displayed in the zoomed-in pictures. Obviously, the GeMnSe film exhibits a polycrystalline structure, which is also verified by the selected area electron diffraction (SAED) pattern in Fig. 2f.

The crystalline structures of the samples were then investigated by XRD patterns and Raman spectra. Fig. 3a shows that obvious diffraction peaks at 26.1°, 30.9°, 32.1°, 33.0°, 39.9°, 40.7°, 45.9°, 47.4°, 48.5°, 50.7°, 52.8°, 54.9°, 58.9°, 74.4°, and 78.4° are observed in all the GeTMSe films, which are similar to the undoped GeSe film. These diffraction peaks are exactly indexed to the (201), (011), (111), (400), (311), (410), (411), (020), (112), (212), (511), (221), (420), (422), and (131) planes of α-GeSe with a *Pnma* space (JCPDS 48-1226), respectively, and no other secondary phases or extraneous impurities are detected [27], indicating that the orthorhombic α-GeSe crystalline structure does not change after TM doping. The zoomed-in XRD patterns in Fig. 3b show that the (111) and (400) peaks of the GeTMSe films all shift to a lower angle with respect to that of undoped GeSe film, and the lattice constants in Fig. 3c obtained from the representative (201), (111) and (400) peaks show that the expansion of the lattice constants is induced by TM doping in the films. The results indicate that TM atoms are successfully incorporated in the GeSe host, as TM atoms with larger ionic radii substituting Ge atoms in the GeSe lattice expand the lattice due to the increase of in-plane chemical pressure. Fig. 3d shows the Raman spectra of the pure GeSe and GeTMSe films. The representative peaks of 145.9, 175.9, 188.3, 198.3, and 258.7 cm^{-1} are observed in the pure GeSe film, exactly corresponding to the vibrational modes B_{3g}, A_g^2, A_g^3, B_{2g}^3, and B_{2g}^2, respectively [28]. Notably, all the GeTMSe films possess two apparent peaks at 175.9 cm^{-1} (A_g^2) and 198.3 cm^{-1} (B_{2g}^3) and a new peak at 289 cm^{-1}, but no peaks at 145.9 cm^{-1} (B_{3g}) and 188.3 cm^{-1} (A_g^3). The disappearance of in-plane vibration modes B_{3g} and A_g^3 in Fig. 3e is because TM atoms are preferentially doped into Ge sites in GeSe lattice rather than in interlayer sites to increase the in-plane chemical pressure in GeTMSe films [29], as depicted in Fig. 3f. The Raman signals at 175.9 cm^{-1} (A_g^2) and 198.3 cm^{-1} (B_{2g}^3) are usually related to the defects induced by intrinsic Ge vacancies (V$_{Ge}$s) in GeSe [29,30]. The seemingly new peak at
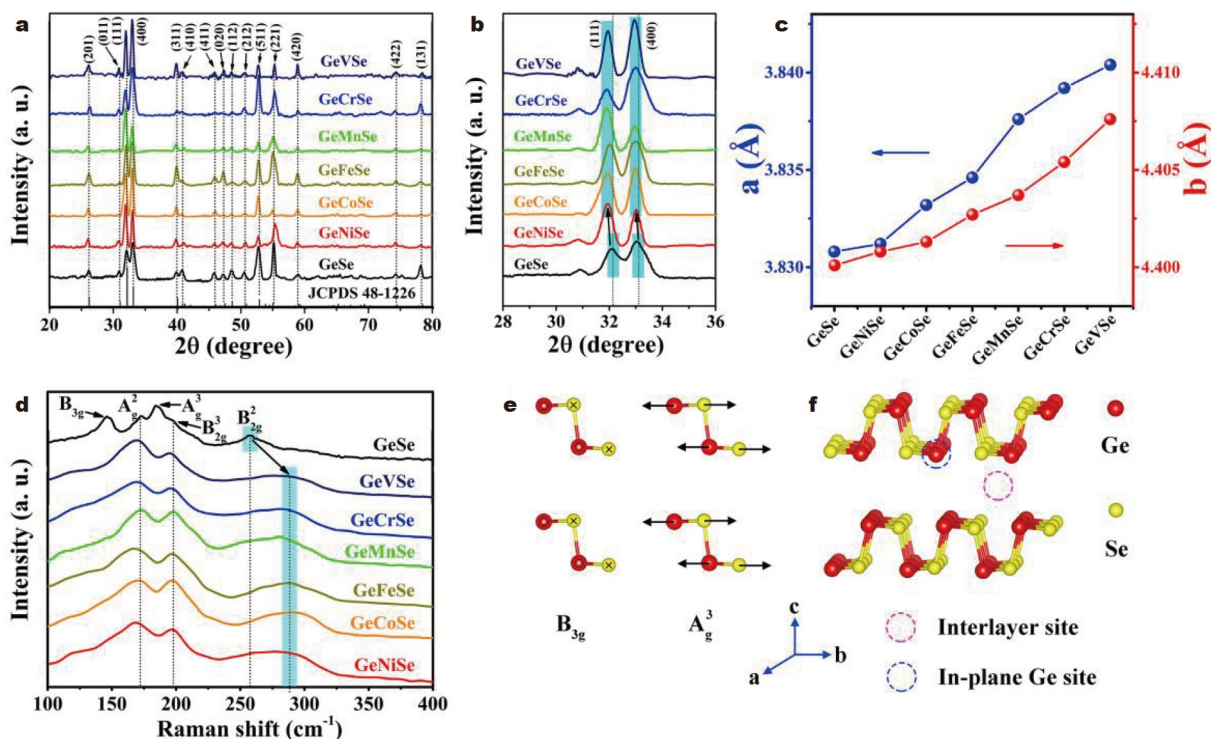

Figure 3 (a) XRD patterns and (b) the zoomed-in segments of the (111) and (400) peaks of the samples. (c) Lattice constants of pure GeSe and GeTMSe films. (d) Raman spectra of pure GeSe and GeTMSe films. (e) Atomic displacements of B_{3g} and A_g^3 vibration modes in GeSe. (f) Schematic of in-plane Ge site in GeSe.

289 cm^{-1} is actually shifted and broadened from the peak at 258.7 cm^{-1} by TM doping, which represents the phonon vibrations of V_{Ge}-induced Se chains and Se–Se bonds [29,31] and indicates the successful incorporation of TM dopants in GeSe host. Here the shift and broadening of the Raman peak at 258.7 cm^{-1} in the GeTMSe films can be clearly observed, which is due to the tensile strain caused by the increase of lattice constant. The increase of lattice constant originates from the incorporation of TM dopants, the formation of intrinsic defects, and the existence of lattice mismatches between the GeSe films and the SiO$_2$/Si substrate. Since the atomic radius of the TM dopants are larger than those of Ge (1.25 Å) and Se (1.22 Å), doping TM dopants in the GeSe lattice results in the increase of the lattice constants (and tensile strain). The intrinsic point defects (V_{Ge}s) are naturally generated in the growth process of GeSe due to their lower formation energies than those of other point defects, which leads to the increase of the lattice constants since most of the defects are Schottky-type defects [32,33]. The lattice mismatch is derived from the discrepancy between the GeTMSe film and the SiO$_2$/Si substrate with a bigger lattice

constant, which further leads to the emergence of tensile strain [34].

Then the magnetization measurements of the GeTMSe films are performed. Fig. 4a, b (and Fig. S7a–d) show the magnetization vs. magnetic field (*M-H*) curves of the samples at 300 K with in-plane and out-of-plane magnetic field applied, respectively. Since all the films exhibit an in-plane easy axis of magnetization, subsequent magnetization measurements were performed with an in-plane field applied up to 3000 Oe. In magnetic thin films, magnetic anisotropy denotes the preferential alignment of the magnetic spins in specified crystal orientations, which usually includes the magneto crystalline anisotropy and the strain-related magnetic anisotropy [35]. Among them, magneto crystalline anisotropy reflects the symmetric crystallographic structure of single crystals. Different from single crystals, polycrystalline thin films have no magnetocrystalline anisotropy due to the randomly oriented grains. If polycrystalline thin films exhibit magnetic anisotropy, their magnetic anisotropy mainly arises from the strain-related anisotropy [36]. In our GeTMSe films, the magnetic anisotropy
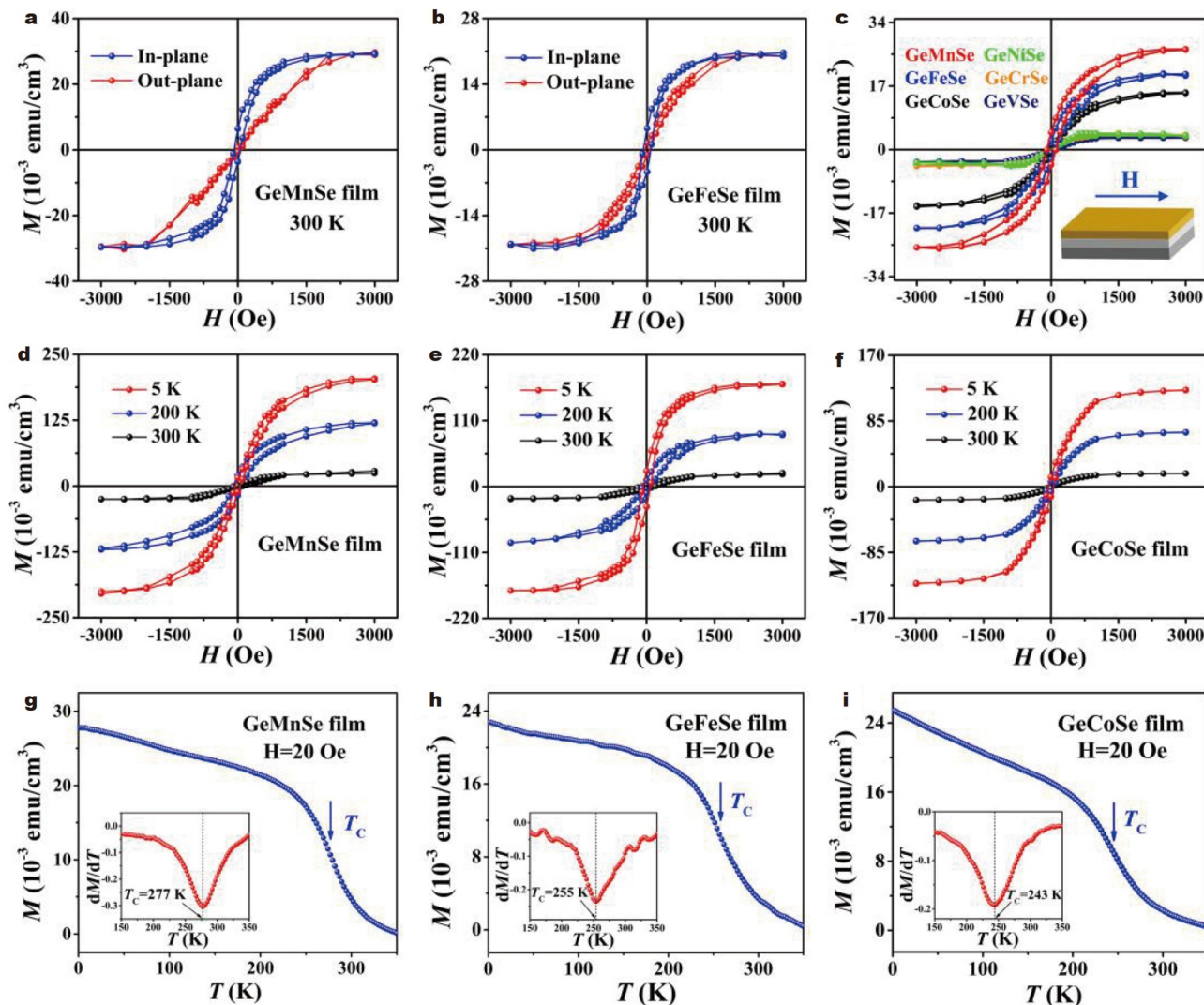

Figure 4 (a, b) *M-H* loops of the GeMnSe and GeFeSe films at 300 K with in-plane and out-of-plane fields applied, respectively. (c) *M-H* loops of the GeTMSe films at 300 K. (d–f) *M-H* loops of the GeMnSe, GeFeSe, and GeCoSe films with in-plane field at 5, 200, and 300 K, respectively. (g–i) *M-T* curves of the GeMnSe, GeFeSe, and GeCoSe films, respectively. The insets show the first derivative of the *M-T* curves.

result from the tensile strain-related magnetic anisotropy due to the increase of lattice constants. Fig. 4c shows the M-H curves under an in-plane applied magnetic field at 300 K, where the diamagnetic signal of the Si/SiO$_2$ substrate is subtracted. It is notable that the Mn-, Fe-, and Co-doped GeSe films exhibit obvious hysteresis loops, and the saturation magnetization (M_S) can reach 2.85×10^{-2}, 2.04×10^{-2} and 1.73×10^{-2} emu cm^{-3}, suggesting the presence of robust FM. Nevertheless, V-, Cr-, and Ni-doped GeSe films show weak FM ($M_S \sim 3.81 \times 10^{-3}$, 4.20×10^{-3} and 4.52×10^{-3} emu cm^{-3}). In the following, we will focus on the GeTMSe (TM = Mn, Fe, and Co) films with robust FM. As shown in Fig. 4d–f, M-H curves of GeTMSe (TM = Mn, Fe, and Co) films at different temperatures exhibit distinct hysteresis loops, indicating ferromagnetic ordering in the samples. Based on the obtained M_S at 5 K and the dopant concentration k through EDS and XPS, the effective magnetic moments can be estimated using M_S/N, where N is the numbers of TM ions and is given by $N = (N_A/M_{TM}) \times k$, in which M_{TM} is the relative atomic weight of TM atom and N_A is the Avogadro constant, respectively. The magnetic moments per Mn, Fe, and Co ions are estimated to 1.2 μ_B, 0.8 μ_B, and 0.5 μ_B at 5 K, respectively, lower than the theoretical results (5.0 μ_B, 4.0 μ_B, and 3.0 μ_B, respectively) reported by Yang et al. [21]. Fig. 4g–i show the M-T curves of GeMnSe, GeFeSe, and GeCoSe films measured with a 20 Oe in-plane field. It is noteworthy that all the M-T curves show a convex behavior in which the magnetizations slowly decrease with increasing temperature, suggesting long-range ferromagnetic interaction in the films. The T_C values can be estimated by the minima of the first derivative of the M-T curves (dM/dT) in Fig. 4g–i, which are 277, 255 and 243 K for GeMnSe, GeFeSe and GeCoSe films, respectively. Among them, GeMnSe film has the maximum M_S (2.85×10^{-2} emu cm^{-3}), T_C (277 K) and magnetic moment (1.2 μ_B), showing great potential as a high-T_C DMS thin film.

Notably, the M-H and M-T measurements indicate no signals of TM clustering in the GeTMSe (TM = Mn, Fe, and Co) films. It is known that ferromagnetic clusters usually result in unsaturated magnetization in M-H curves at high fields [37], whereas the GeTMSe films exhibit typical signals of saturation magnetization (Fig. 4d–f). In addition, short-range ferromagnetic order caused by TM clusters often results in a concave M-T behavior in IV-VI DMSs [1], which is not observed in the M-T curves of the GeTMSe films (Fig. 4g–i). Furthermore, no characteristic magnetic signals of MnSe, FeSe, CoSe, MnGe, FeGe, and CoGe phases are observed in our samples. MnSe usually shows paramagnetic [38] and antiferromagnetic [39] behaviors at low temperatures, whereas our GeMnSe films have obvious ferromagnetic properties in the whole temperature range from 5 to 300 K. FeSe shows a larger coercivity (H_C) between 300 and 2000 Oe and exhibits an antiferromagnetic ordering below 150 K [40], neither of which is observed in the GeFeSe films. CoSe usually has larger H_C between 350 and 600 Oe in the temperature range of 5~300 K [41], whereas our GeCoSe films have much lower H_C of ~100 Oe at 5 K. Typical MnGe compounds such as Mn$_5$Ge$_3$ and Mn$_{11}$Ge$_8$ exhibit their own characteristic magnetic signals. Mn$_5$Ge$_3$ usually shows a transition from FM to superparamagnetism at 210 K and Mn$_{11}$Ge$_8$ exhibits an antiferromagnetic ordering below 150 K [42], both of which are not found in our GeMnSe films. Furthermore, these MnGe compounds usually have larger H_C between 1260~2000 Oe at 180 K [43] and ~1000 Oe at 5 K [44], whereas our GeMnSe films have much lower H_C of about 100 Oe at 5 K. FeGe usually shows a larger H_C of 528 Oe at 5 K [45], whereas our GeFeSe films have much lower H_C of ~100 Oe at 5 K. CoGe is usually a Pauli paramagnet [46], whereas our GeCoSe films exhibit ferromagnetic properties.

The local electronic and spintronic structures of Mn, Fe, and Co ions in the samples were studied by XPS and EPR spectra. Fig. 5a–c show the XPS spectra of the Mn 2p, Fe 2p, and Co 2p. Here the Shirley model was used for background subtraction
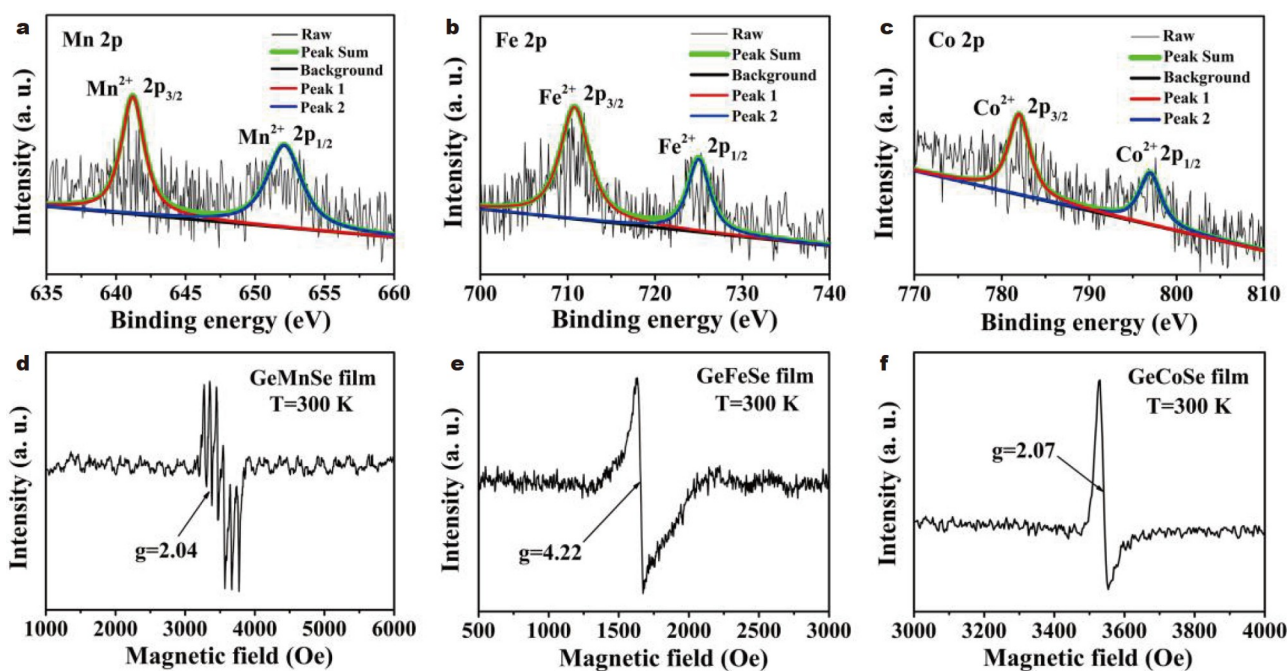

Figure 5 (a) Mn 2p spectra of GeMnSe film. (b) Fe 2p spectra of GeFeSe film. (c) Co 2p spectra of GeCoSe film. Typical EPR spectrum of (d) GeMnSe film, (e) GeFeSe film, and (f) GeCoSe film measured at RT.

and a mixed Gaussian-Lorentzian function was used in the fitting process [47]. The Mn 2p spectrum in Fig. 5a shows two main peaks at ~641.24 and ~652.07 eV, which can be assigned to the Mn^{2+} valence state [1] in the GeMnSe film. The Fe 2p spectrum in Fig. 5b shows two major peaks at ~710.81 and ~724.02 eV, which are identified as the Fe^{2+} valence state [48] in the GeFeSe films. The Co 2p spectrum in Fig. 5c shows two typical peaks for Co $2p_{3/2}$ (781.56 eV) and Co $2p_{1/2}$ (797.17 eV), indicating the Co^{2+} valence state in the GeCoSe film [49]. The collected XPS signals of TM atoms are noisy owing to the low TM concentrations (~1.0%), similar to the results in 8.0% Mn-doped GeTe epilayers [1]. The EPR spectra of the films are shown in Fig. 5d–f. Fig. 5d shows strong axially distorted six hyperfine lines with separation of 9.00 mT, consistent with the room-temperature hyperfine six-line EPR spectra Mn^{2+} ($S = 5/2$) [50]. In addition, the g-factor at RT is 2.04, which is in the range

of $g = 2.02$–2.07 for Mn^{2+} in Mn-doped GeTe [51]. Fig. 5e shows an intensive signal at 1684 Oe and the effective g-factor (g_{eff}) of 4.22, both of which correspond to magnetic Fe^{2+} ($S = 3/2$) ions [52]. Fig. 5f shows an intense sharp signal ($g_{eff} \sim 2.07$) at 3527 Oe, corresponding to magnetic Co^{2+} ($S = 3/2$) ions [53]. These characteristic EPR spectra exhibit that the magnetic signals are mainly attributed to spin configurations of the TM ions, including Mn^{2+} ($3d^5$ $S = 5/2$), Fe^{2+} ($3d^6$ $S = 3/2$) and Co^{2+} ($3d^6$ $S = 3/2$).

The electrical and magnetic properties of GeTMSe (TM = Mn, Fe, and Co) films were investigated by magneto-transport measurements. The configurations of the van der Pauw devices used for the measurements are shown in Fig. 6a (and Fig. S8). Fig. 6b shows the temperature-dependent resistivity (ρ-T) curves for the films without magnetic field, where ρ increases sharply with the decrease of temperature when $T \leq 20$ K, indicating
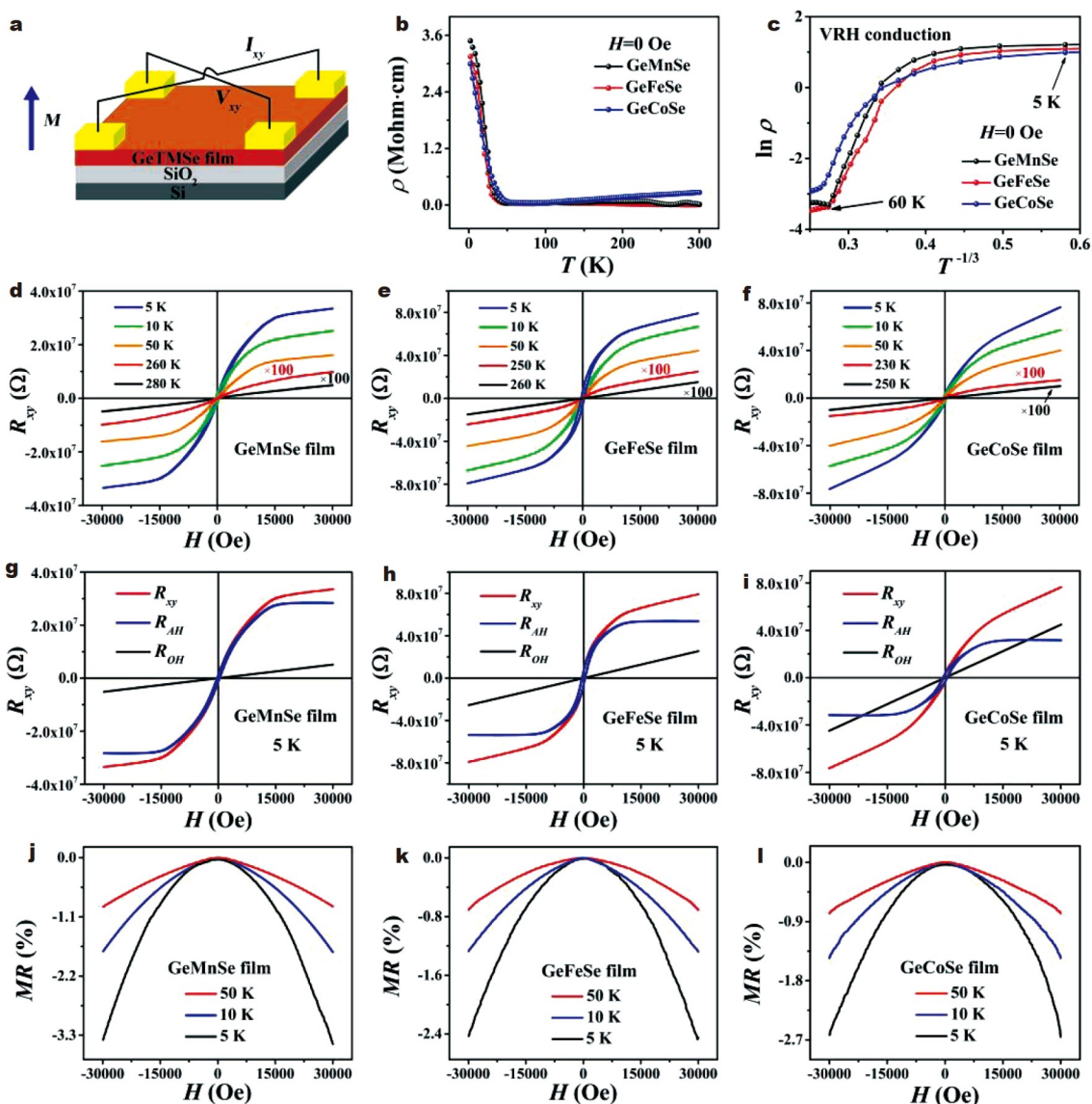

Figure 6 (a) Measurement configuration of van der Pauw method. (b) Temperature dependence of the resistivity of GeTMSe (TM = Mn, Fe, and Co) films between 5 and 300 K. (c) The resistivity on a natural logarithmic scale as a function of $T^{-1/3}$ at 0 Oe field. (d–f) R_{xy}-H curves of GeTMSe (TM = Mn, Fe, and Co) films at different temperatures with a magnetic field perpendicular to the film surface. (g–i) R_{xy}-H curves and decomposed anomalous R_{AH} and ordinary R_{OH} of GeTMSe (TM = Mn, Fe, and Co) films at 5 K. (j–l) Normalized MR curves of GeTMSe (TM = Mn, Fe, and Co) films at different temperatures.

semiconducting characteristics of the GeTMSe films. This rapid increase of ρ at low temperatures probably originates from the Coulomb gap caused by the strong electron-electron interaction. The ρ-T curves are fitted using the function of $\rho = \rho_0 \exp(T^{-1/n})$, where n equals to 2, 3, or 4 and ρ_0 is the pre-exponential factor. As shown in Fig. 6c, when $n = 3$, the best least square fit is obtained and obvious Mott-type variable range hopping (VRH) conduction [54] at the temperature range of 5~60 K is observed, which is similar to what was observed in GeMnTe films [55]. The conduction mechanism can be understood as follows. In the polycrystalline GeTMSe films, random scattering centers originated from homogeneous distribution of imperfections, such as intrinsic V_{Ge}s, TM dopants and grain boundaries, are responsible for the formation of localized energy states in the forbidden band gap of carriers [56]. When the energy of hole carriers exceeds the energy difference between localized states, hole carriers will transfer and hop among the localized states [55], resulting in the Mott-type VRH conduction. Therefore, the conduction behavior again indicates the co-existence of TM dopants and carriers (holes) induced by V_{Ge}s in the GeTMSe films, consistent with the Raman and EDS mapping results abovementioned.

To determine the carrier types and carrier concentrations of these films, the magnetic field dependence of Hall resistance (R_{xy}) at different temperatures was measured. In Fig. 6d–f, all the R_{xy}-H curves show positive slopes, indicating that the hole is the majority carrier in the GeTMSe films. In addition, anomalous Hall effect (AHE) below T_C is observed in these films, consistent with the results of FM in the films revealed by the magnetization measurements in Fig. 4. In ferromagnetic materials, R_{xy} can be expressed as $R_{xy} = R_0 \cdot B \cdot d^{-1} + R_S \cdot M \cdot d^{-1}$, where R_0 and R_S are the ordinary and anomalous Hall coefficients, respectively, B is the magnetic induction, d is the film thickness, and M is the magnetization perpendicular to the film [57]. The linear ordinary Hall term $R_0 B d^{-1}$-H and the anomalous Hall conductivity $R_S M d^{-1}$-H are extracted from R_{xy}-H curves under a high magnetic field, and plotted in Fig. 6g–i. Based on the slope of $R_0 B d^{-1}$-H curves, the carrier (hole) concentrations of GeMnSe, GeFeSe, and GeCoSe films are estimated to be 4.60×10^{19}, 9.19×10^{18}, and 6.33×10^{18} cm^{-3} at 5 K, respectively, which may enhance the FM in these films due to the carrier-enhanced RKKY interaction [15,57]. As a typical example, the magnetization measurements of the GeFeSe films with different carrier concentrations (Fig. S9) show that both M_S and T_C increase with increasing carrier concentration, suggesting the presence of carrier-enhanced FM in the samples. The hole concentrations in the GeTMSe films reach $\sim 10^{20}$ cm^{-3} at 300 K (Table S1). The
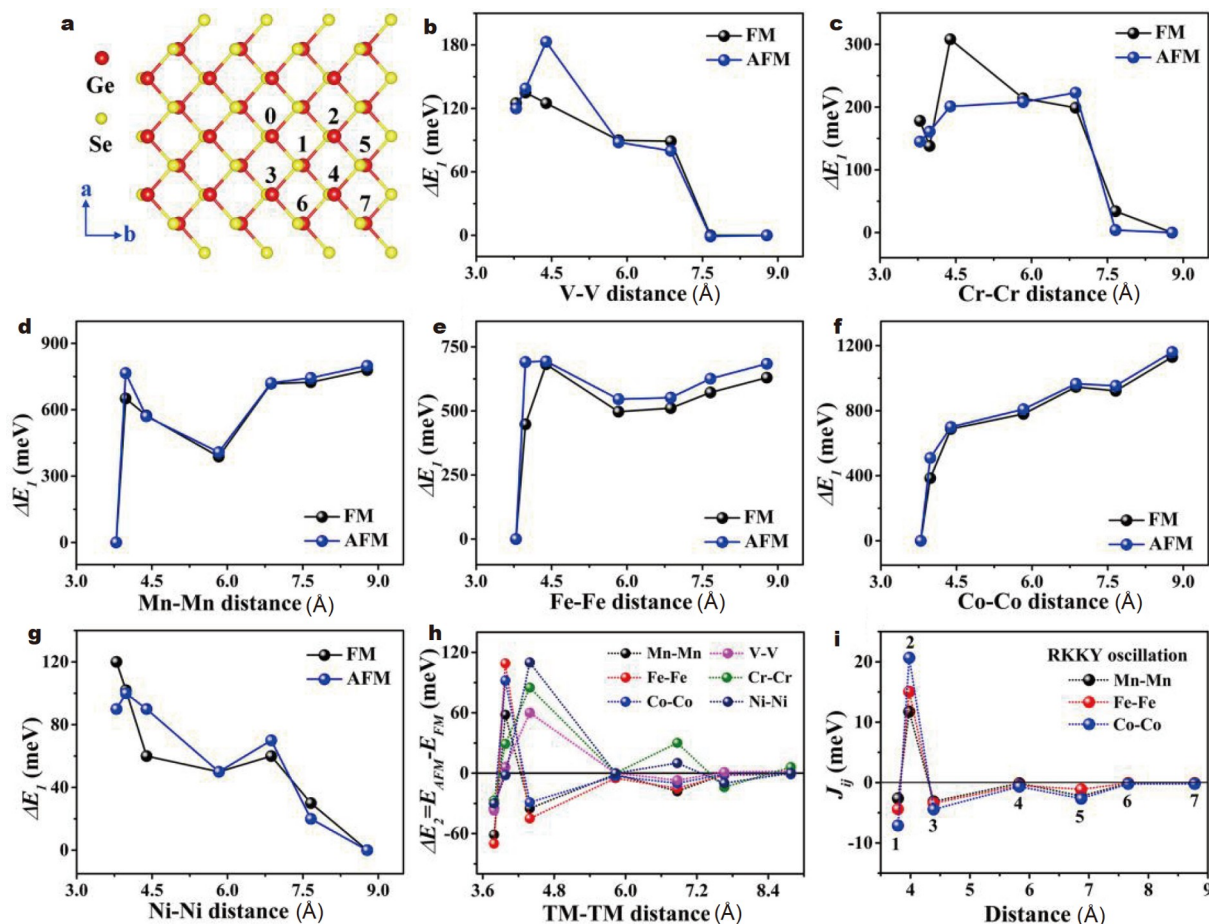

Figure 7 (a) The atomic structure of GeTMSe, where Ge atoms at site 0 and at site j (1–7) are substituted by TM atoms. Red (yellow) spheres designate Ge (Se) atoms. (b–g) The relative energies (ΔE_1) of seven different configurations as the TM-TM distance changes for both AFM and FM states, respectively. The total energy of the ground state in each GeTMSe is set as zero. (h) The energy difference (ΔE_2) between the AFM and FM configuration of seven different configurations. (i) The effective exchange interactions J_{ij} between substitutional TM atom pairs as a function of interatomic distance.

abundant holes are induced by easily formed V_{Ge}s owing to their smaller formation energies during the GeSe growth process [33]. The normalized magnetoresistance (MR) ratio is defined as MR $= (R_{xx}(H) - R_{xx}(0))/(R_{xx}(0))$, where the $R_{xx}(H)$ and $R_{xx}(0)$ are the resistances with and without applied field, respectively [55]. Fig. 6j–l show the magnetic field-dependent MR ratios in these GeTMSe films at given temperatures, where negative MR is observed. The MR ratio values decrease monotonically with increasing magnetic field and show a linear and non-saturating behavior, consistent with previous results in IV-VI DMSs [58]. This unsaturated linear negative MR is a general signal in ferromagnetic materials, which can be ascribed to the spin disorder scattering [59] originated from the vacancies, interstitials and grain boundaries in our polycrystalline GeTMSe films.

In order to understand the diversity of the FM behaviors in different GeTMSe films, the distributions of TM atoms in the GeSe lattice are theoretically analyzed first. To simplify the simulation, a $3 \times 4 \times 1$ supercell of GeSe is utilized, in which two Ge atoms are replaced by TM atoms (TM = V, Cr, Mn, Fe, Co, and Ni) and the TM doping concentration is about 4.2%. Specifically, one TM atom is placed at a Ge site (labeled as 0 in Fig. 7a), and the other TM atom is placed at one of the positions labeled as j (1–7) of Ge sites according to the variation of TM-TM distance. According to the periodicity and the symmetry, seven possible different configurations are considered and the relative energies (ΔE_1) of both ferromagnetic and antiferromagnetic states are calculated for each TM doping, as shown in Fig. 7b–g. Here, ΔE_1 is determined by $\Delta E_1 = E_j - E_0$ ($j = 1$–7), where E_0 denotes the ground state energy of the seven configurations. It is obvious that the Mn, Fe and Co atoms tend to be distributed with closer TM–TM distances, while V, Cr and Ni atoms tend to be distributed with larger TM–TM distances. According to the structural and magnetization characterizations, no TM clustering has been observed in the GeTMSe films, which is probably related to the facts that TM doping concentration is not high and the grain boundaries of poly-crystalline GeTMSe systems may restrain the TM atoms from moving closely to form clustering. Therefore, despite that the DFT calculations of single-crystalline GeTMSe (TM = Mn, Fe, Co) systems indicate that the TM atoms energetically prefer to be close to each other, the

experimental measurements show that the Mn, Fe, and Co atoms are distributed without formation of TM clustering in the GeSe host. Due to the interplay between the delocalized carriers spins and the localized spins of the TM ions, the TM atoms in the GeTMSe films are more likely to be coupled indirectly via sufficient hole carriers, resulting in carrier-induced RKKY interaction, which is similar to those in other IV-VI DMSs [60]. Owing to the closer TM–TM distances and high hole concentrations in Mn-, Fe-, and Co-doped GeSe films, the carrier-induced RKKY interaction is strengthened and the robust high-T_C FM is obtained [57]. However, the RKKY interaction in V-, Cr-, and Ni-doped GeSe films is weak due to the larger TM–TM distances, leading to weak FM. The substitutional V, Cr, Mn, Fe, Co and Ni dopants in GeSe lattice could introduce magnetic moments of 3.0 μ_B, 4.0 μ_B, 5.0 μ_B, 4.0 μ_B, 3.0 μ_B and 2.0 μ_B per TM ion (Fig. S10), respectively, consistent with previous theoretical results [21].

To further investigate the RKKY interaction in the GeTMSe films, the total energy difference ($\Delta E_2 = E_{AFM} - E_{FM}$) between ferromagnetic (FM) and antiferromagnetic (AFM) states for seven configurations are calculated and shown in Fig. 7h. The ΔE_2 oscillates with rapidly decreasing amplitude as the TM–TM distance increases, indicating a RKKY oscillation. In magnetic systems, the effective classical Heisenberg model is commonly used to study the magnetic order and can be written as $H = -\sum_{(i \neq j)} J_{ij} \mathbf{e}_i \cdot \mathbf{e}_j$, where $\mathbf{e}_i(\mathbf{e}_j)$ is the unit vector of magnetic moment at site $i(j)$, and J_{ij} is the exchange interaction between two TM sites (i, j) [61]. In the GeTMSe (TM = Mn, Fe, and Co) systems, the J_{ij} values without hole mediation are obtained from the formula $J_{ij} = \Delta E_2/2S^2$ [62], where S are assumed to be 5/2 (Mn^{2+}), 3/2 (Fe^{2+}), and 3/2 (Co^{2+}) since EPR results show that the magnetic signals are mainly attributed to Mn^{2+}, Fe^{2+}, and Co^{2+}, respectively. Fig. 7i shows the magnitude of J_{ij} exhibiting a typical RKKY-type oscillation behavior, which will be strengthened by the mediation of holes to induce robust high-T_C FM in IV-VI DMSs [57,58]. The theoretical values of magnetic moments per Mn, Fe and Co dopant (Fig. S10) are larger than those of experimental findings, probably owing to the existence of various defects such as vacancies, interstitials, and grain boundaries of TM magnetic moments [63]. It is worthwhile

Table 1 Summary of experimental results in IV-VI DMS thin films

Samples	T_C (K)	Magnetic moment (μ_B)	Preparation method	Ref.
GeMnTe	190	–	MBE	[1]
GeCrTe	180	1.23 (5 K)	MBE	[14]
GeFeTe	160	–	PLD	[15]
GeMnTe	90	2.95 (4 K)	Vertical Bridgman	[51]
GeMnTe	135	0.72 (5 K)	MBE	[55]
GeMnTe	95	0.11 (5 K)	MBE	[64]
GeMnTe	60	1.14 (4 K)	ICB	[57]
GeMnTe	110	0.159 (5 K)	MBE	[65]
GeMnTe	200	–	MBE	[66]
GeFeTe	170	–	PLD	[67]
GeMnSe	277	1.20 (5 K)	CVD	This work
GeFeSe	255	0.80 (5 K)	CVD	This work
GeCoSe	243	0.50 (5 K)	CVD	This work

noting that the GeMnSe film exhibits the strongest FM in these samples, which is consistent with the theoretical prediction that Mn dopants induce the largest magnetic moment (5 μ_B) than other TM dopants in the GeSe host. However, the GeMnSe films exhibit a lower T_C than Mn-doped GeSe nanocombs owing to the lack of size confinement effects in the films [24].

CONCLUSIONS

In conclusion, GeTMSe (TM = V, Cr, Mn, Fe, Co and Ni) thin films have been fabricated through a facile CVD method and their structural, magnetic and magneto-transport properties are systematically studied. Among them, Mn, Fe and Co-doped GeSe films exhibit robust FM with T_C up to 277, 255 and 243 K, respectively, owing to the carrier-enhanced RKKY indirect interaction in the samples. For comparison, the ferromagnetic properties (T_C and magnetic moment) and preparation methods of a series of 2D IV-VI DMS thin films are listed in Table 1 [1,14,15,51,55,57,64–67]. Our results give a broad horizon on the correlation between the structure and the high-T_C FM in TM-doped GeSe films, which is valuable for fundamental study and practical application of GeSe-based spintronic materials and devices.

1. Fukuma Y, Asada H, Miyawaki S, et al. Carrier-induced ferromagnetism in Ge$_{0.92}$Mn$_{0.08}$Te epilayers with a Curie temperature up to 190 K. Appl Phys Lett, 2008, 93: 777

2. Dietl T, Ohno H. Dilute ferromagnetic semiconductors: Physics and spintronic structures. Rev Mod Phys, 2014, 86: 187–251

3. Park S, Kim P, Lee YP, et al. Realization of room-temperature ferromagnetism and of improved carrier mobility in Mn-doped ZnO film by oxygen deficiency, introduced by hydrogen and heat treatments. Adv Mater, 2007, 19: 3496–3500

4. Chen L, Yang X, Yang F, et al. Enhancing the Curie temperature of ferromagnetic semiconductor (Ga,Mn)As to 200 K via nanostructure engineering. Nano Lett, 2011, 11: 2584–2589

5. Liu W, Zhang H, Shi J, et al. A room-temperature magnetic semiconductor from a ferromagnetic metallic glass. Nat Commun, 2016, 7: 13497

6. Wang H, Sun S, Lu J, et al. High Curie temperature ferromagnetism and high hole mobility in tensile strained Mn-doped SiGe thin films. Adv Funct Mater, 2020, 30: 2002513

7. Shen L, Zhang X, Wang J, et al. Mn-doped SiGe thin films grown by UHV/CVD with room-temperature ferromagnetism and high hole mobility. Sci China Mater, 2022, 65: 2826–2832

8. Wolf SA, Awschalom DD, Buhrman RA, et al. Spintronics: A spin-based electronics vision for the future. Science, 2001, 294: 1488–1495

9. Dietl T. A ten-year perspective on dilute magnetic semiconductors and oxides. Nat Mater, 2010, 9: 965–974

10. Li X, Yang J. Realizing two-dimensional magnetic semiconductors with enhanced curie temperature by antiaromatic ring based organometallic frameworks. J Am Chem Soc, 2018, 141: 109–112

11. Story T, Gałazka RR, Frankel RB, et al. Carrier-concentration-induced ferromagnetism in PbSnMnTe. Phys Rev Lett, 1986, 56: 777–779

12. Nadolny AJ, Sadowski J, Taliashvili B, et al. Carrier induced ferromagnetism in epitaxial Sn$_{1−x}$Mn$_x$Te layers. J Magn Magn Mater, 2002, 248: 134–141

13. Li B, Xing T, Zhong M, et al. A two-dimensional Fe-doped SnS$_2$ magnetic semiconductor. Nat Commun, 2017, 8: 1958

14. Fukuma Y, Asada H, Moritake N, et al. Ferromagnetic semiconductor Ge$_{1−x}$Cr$_x$Te with a Curie temperature of 180 K. Appl Phys Lett, 2007, 91: 092501

15. Liu JD, Miao XS, Tong F, et al. Ferromagnetism and electronic transport in epitaxial Ge$_{1−x}$Fe$_x$Te thin film grown by pulsed laser deposition.

Appl Phys Lett, 2013, 102: 102402

16. Ma S, Li G, Li Z, et al. 2D magnetic semiconductor Fe$_3$GeTe$_2$ with few and single layers with a greatly enhanced intrinsic exchange bias by liquid-phase exfoliation. ACS Nano, 2022, 16: 19439–19450

17. Gong C, Li L, Li Z, et al. Discovery of intrinsic ferromagnetism in two-dimensional van der Waals crystals. Nature, 2017, 546: 265–269

18. Lin MW, Zhuang HL, Yan J, et al. Ultrathin nanosheets of CrSiTe$_3$: A semiconducting two-dimensional ferromagnetic material. J Mater Chem C, 2016, 4: 315–322

19. Zhuang HL, Xie Y, Kent PRC, et al. Computational discovery of ferromagnetic semiconducting single-layer CrSnTe$_3$. Phys Rev B, 2015, 92: 035407

20. Sivadas N, Daniels MW, Swendsen RH, et al. Magnetic ground state of semiconducting transition-metal trichalcogenide monolayers. Phys Rev B, 2015, 91: 235425

21. Yang L, Wu M, Yao K. Transition-metal-doped group-IV monochalcogenides: A combination of two-dimensional triferroics and diluted magnetic semiconductors. Nanotechnology, 2018, 29: 215703

22. Mao Y, Guo G, Yuan J, et al. Edge-doping effects on the electronic and magnetic properties of zigzag germanium selenide nanoribbon. Appl Surf Sci, 2019, 464: 236–242

23. Shu Z, Cai Y. Substitutional doped GeSe: Tunable oxidative states with strain engineering. J Mater Chem C, 2020, 8: 13655–13667

24. Li D, Zhang X, He W, et al. Structure-dependent high-T_C ferromagnetism in Mn-doped GeSe. Nanoscale, 2022, 14: 13343–13351

25. Kresse G, Furthmüller J. Efficient iterative schemes for ab initio total-energy calculations using a plane-wave basis set. Phys Rev B, 1996, 54: 11169–11186

26. Zhao Y, Zhang Y, Yan P, et al. Increasing the photocatalytic properties of monolayer black phase GeSe by 3d transition metal doping: From ultraviolet to infrared absorption. Mol Catal, 2020, 496: 111195

27. Wang X, Li Y, Huang L, et al. Short-wave near-infrared linear dichroism of two-dimensional germanium selenide. J Am Chem Soc, 2017, 139: 14976–14982

28. Ribeiro HB, Ramos SLLM, Seixas L, et al. Edge phonons in layered orthorhombic GeS and GeSe monochalcogenides. Phys Rev B, 2019, 100: 094301

29. Bellin C, Pawbake A, Paulatto L, et al. Functional monochalcogenides: Raman evidence linking properties, structure, and metavalent bonding. Phys Rev Lett, 2020, 125: 145301

30. Li X, Zhang X, Lv X, et al. Synthesis and photoluminescence of high density GeSe triangular nanoplate arrays on Si substrates. Nanotechnology, 2020, 31: 285702

31. Jackson K, Briley A, Grossman S, et al. Raman-active modes of a-GeSe$_2$ and a-GeS$_2$: A first-principles study. Phys Rev B, 1999, 60: R14985–R14989

32. Wiedigen S, Kramer T, Feuchter M, et al. Interplay of point defects, biaxial strain, and thermal conductivity in homoepitaxial SrTiO$_3$ thin films. Appl Phys Lett, 2012, 100: 061904

33. He T, Wang Z, Cao R, et al. Extrinsic photoconduction induced short-wavelength infrared photodetectors based on Ge-based chalcogenides. Small, 2021, 17: 2006765

34. Liu G, Wu L, Chen X, et al. The investigations of characteristics of GeSe thin films and selector devices for phase change memory. J Alloys Compd, 2019, 792: 510–518

35. Boschker H, Mathews M, Houwman EP, et al. Strong uniaxial in-plane magnetic anisotropy of (001)- and (011)-oriented La$_{0.67}$Sr$_{0.33}$MnO$_3$ thin films on NdGaO$_3$ substrates. Phys Rev B, 2009, 79: 214425

36. Kumar D, Singh S, Vishawakarma P, et al. Tailoring of in-plane magnetic anisotropy in polycrystalline cobalt thin films by external stress. J Magn Magn Mater, 2016, 418: 99–106

37. Kumar A, Tandon RP, Awana VPS. Study of spin glass and cluster ferromagnetism in RuSr$_2$Eu$_{1.4}$Ce$_{0.6}$Cu$_2$O$_{10−δ}$ magneto superconductor. J Appl Phys, 2011, 110: 043926

38. Zhou B, Yang X, Sui Y, et al. Alternative motif toward high-quality wurtzite MnSe nanorods via subtle sulfur element doping. Nanoscale, 2016, 8: 8784–8790

39. Chen CC, Hsu YJ, Lin YF, et al. Superparamagnetism found in diluted magnetic semiconductor nanowires: Mn-doped CdSe. J Phys Chem C,

2008, 112: 17964–17968

40 Takemura Y, Suto H, Honda N, *et al.* Characterization of FeSe thin films prepared on GaAs substrate by selenization technique. J Appl Phys, 1997, 81: 5177–5179

41 Zhang M, Liu L, Yang H. Anomalous second ferromagnetic phase transition in $Co_{0.08}Bi_{1.92}Se_3$ topological insulator. J Alloys Compd, 2016, 678: 463–467

42 Jaeger C, Bihler C, Vallaitis T, *et al.* Spin-glass-like behavior of Ge:Mn. Phys Rev B, 2006, 74: 045330

43 Cho S, Choi S, Hong SC, *et al.* Ferromagnetism in Mn-doped Ge. Phys Rev B, 2002, 66: 033303

44 Zeng C, Erwin SC, Feldman LC, *et al.* Epitaxial ferromagnetic Mn_5Ge_3 on Ge(111). Appl Phys Lett, 2003, 83: 5002–5004

45 Wu WY, Tjiu WW, Wan W, *et al.* Endotaxial growth of Fe_xGe single-crystals on Ge(001) substrates. CrystEngComm, 2018, 20: 2916–2922

46 Tsvyashchenko AV, Sidorov VA, Fomicheva LN, *et al.* High pressure synthesis and magnetic properties of Cubic B20 MnGe and CoGe. Solid State Phenom, 2012, 190: 225–228

47 Shirley DA. High-resolution X-ray photoemission spectrum of the valence bands of gold. Phys Rev B, 1972, 5: 4709–4714

48 Cai SH, Chen XN, Huang MJ, *et al.* Interfacial engineering of nickel/iron/ruthenium phosphides for efficient overall water splitting powered by solar energy. J Mater Chem A, 2022, 10: 772–778

49 Sun XJ, Yang DD, Dong H, *et al.* ZIF-derived CoP as a cocatalyst for enhanced photocatalytic H_2 production activity of $g-C_3N_4$. Sustain Energy Fuels, 2018, 2: 1356–1361

50 Reddy AJ, Kokila MK, Nagabhushana H, *et al.* EPR and photoluminescence studies of ZnO:Mn nanophosphors prepared by solution combustion route. Spectrochim Acta Part A-Mol Biomol Spectr, 2011, 79: 476–480

51 Zvereva EA, Savelieva OA, Primenko AE, *et al.* Anomalies in electron spin resonance spectra of $Ge_{1-x}Mn_xTe$ diluted magnetic semiconductors. J Appl Phys, 2010, 108: 093923

52 Misra SK, Andronenko SI, Thurber A, *et al.* An X- and Q-band Fe^{3+} EPR study of nanoparticles of magnetic semiconductor $Zn_{1-x}Fe_xO$. J Magn Magn Mater, 2014, 363: 82–87

53 Li C, Lou X, Shen M, *et al.* High-capacity cobalt-based coordination polymer nanorods and their redox chemistry triggered by delocalization of electron spins. Energy Storage Mater, 2017, 7: 195–202

54 Efros AL, Shklovskii BI. Coulomb gap and low temperature conductivity of disordered systems. J Phys C-Solid State Phys, 1975, 8: L49–L51

55 Chen WQ, Lim ST, Sim CH, *et al.* Optical, magnetic, and transport behaviors of $Ge_{1-x}Mn_xTe$ ferromagnetic semiconductors grown by molecular-beam epitaxy. J Appl Phys, 2008, 104: 063912

56 Shah M, Nadeem M, Atif M. Dielectric relaxation with polaronic and variable range hopping mechanisms of grains and grain boundaries in $Pr_{0.8}Ca_{0.2}MnO_3$. J Appl Phys, 2012, 112: 103718

57 Fukuma Y, Asada H, Arifuku M, *et al.* Carrier-enhanced ferromagnetism in $Ge_{1-x}Mn_xTe$. Appl Phys Lett, 2002, 80: 1013–1015

58 Lim ST, Bi JF, Hui L, *et al.* Exchange interaction and Curie temperature in $Ge_{1-x}Mn_xTe$ ferromagnetic semiconductors. J Appl Phys, 2011, 110: 023905

59 Wang X, Bian C, He Y, *et al.* Ultrathin FeTe nanosheets with tetragonal and hexagonal phases synthesized by chemical vapor deposition. Mater Today, 2021, 45: 35–43

60 Fukuma Y, Arifuku M, Asada H, *et al.* Correlation between magnetic properties and carrier concentration in $Ge_{1-x}Mn_xTe$. J Appl Phys, 2002, 91: 7502–7504

61 Sato K, Bergqvist L, Kudrnovský J, *et al.* First-principles theory of dilute magnetic semiconductors. Rev Mod Phys, 2014, 82: 1633–1690

62 Lan M, Xiang G, Zhang X. Electronic structures and magnetic stabilities of 2D Mn-doped GaAs nanosheets: The role of long-range exchange interactions and doping strategies. J Appl Phys, 2014, 116: 083912

63 Wen Y, Liu Z, Zhang Y, *et al.* Tunable room-temperature ferromagnetism in two-dimensional Cr_2Te_3. Nano Lett, 2020, 20: 3130–3139

64 Chen WQ, Teo KL, Lim ST, *et al.* Magnetic and transport behaviors in $Ge_{1-x}Mn_xTe$ with high Mn composition. Appl Phys Lett, 2007, 90: 142514

65 Chen WQ, Teo KL, Jalil MBA, *et al.* Compositional dependencies of ferromagnetic $Ge_{1-x}Mn_xTe$ grown by solid-source molecular-beam epitaxy. J Appl Phys, 2006, 99: 08D515

66 Hassan M, Springholz G, Lechner RT, *et al.* Molecular beam epitaxy of single phase GeMnTe with high ferromagnetic transition temperature. J Cryst Growth, 2011, 323: 363–367

67 Liu J, Cheng X, Tong F, *et al.* Spin-glass behavior and anomalous magnetoresistance in ferromagnetic $Ge_{1-x}Fe_xTe$ epilayer. J Appl Phys, 2014, 116: 043901

Author contributions Li D prepared the samples and performed the experiments; Zhang X, He W, and Peng Y provided the resources and supervised the project; Li D, Zhang X, and Xiang G wrote the paper; Xiang G designed and supervised the project. All authors contributed to the general discussion.

Conflict of interest The authors declare that they have no conflict of interest.

Supplementary information Supporting data are available in the online version of the paper.

Deren Li is a PhD student at Sichuan University under the supervision of Prof. Gang Xiang. His current research interests focus on the IV-VI diluted magnetic semiconductors as well as the related functional devices.

Gang Xiang earned his PhD degree in condensed matter physics from Pennsylvania State University-University Park in 2006. Then he worked at Pennsylvania State University-University Park (2006–2007) and also at Ohio State University-Columbus (2007–2010) as a postdoctoral researcher. He joined Sichuan University in 2010. His research interests include the design and fabrication of novel magnetic materials and semiconductors, and their spintronic and electronic applications.

过渡金属(TM = V, Cr, Mn, Fe, Co, Ni)掺杂GeSe的高温铁磁半导体薄膜

李德仁[1], 张析[1*], 何文杰[1], 彭勇[2], 向钢[1*]

摘要 具有高温铁磁性的IV族金属硫族化物磁性半导体薄膜是半导体自旋电子器件所需要的重要材料. 本文采用固体源化学气相沉积法制备了一系列过渡金属元素(TM = V, Cr, Mn, Fe, Co和Ni)掺杂GeSe的多晶半导体薄膜样品. 磁性测量表明, Mn, Fe和Co掺杂的GeSe薄膜表现出较强的铁磁性, 居里温度(T_C)分别高达277, 255和243 K, 而V, Cr和Ni掺杂GeSe的多晶薄膜表现出较弱的铁磁性. 磁电输运测量表明, Mn, Fe和Co掺杂GeSe的多晶薄膜具有相对较高的空穴浓度, 在300 K下高达~10^{20} cm^{-3}. 基于实验和计算结果的进一步分析表明, Mn, Fe和Co掺杂GeSe的多晶薄膜中的强铁磁性归因于载流子增强的Ruderman-Kittel-Kasuya-Yosida相互作用. 我们的研究结果展示了过渡金属掺杂GeSe的磁性半导体薄膜的丰富多样性, 并为相关基础研究和器件应用提供了一个新平台.